J Appl Electrochem (2015) 45:217–224
DOI 10.1007/s10800-015-0787-2

RESEARCH ARTICLE

One-step synthesis of self-supporting tin oxide/graphene electrodes for lithium ion batteries

Arthur N. Gildea · Dan Wang · Gerardine G. Botte

Received: 13 July 2014 / Accepted: 24 January 2015 / Published online: 3 February 2015

Abstract A self-supporting binder-free tin oxide (SnO_2) graphene nanocomposite electrode was synthesized through a novel one step solvothermal treatment of graphene oxide (GO) paper. To characterize this electrode X-ray Diffraction, Scanning Electron Microscopy, Atomic Force Microscopy, Raman spectroscopy, Energy-dispersive X-ray spectroscopy, cyclic voltammetry, and constant current galvanic cycling were performed. The solvothermal treatment simultaneously coats amorphous carbon and SnO_2 nanoparticles onto the surface of GO paper, while reducing the GO nanosheets to graphene nanosheets (GNS). This creates a SnO_2/GNS film that is flexible, free-standing, and can be used as the negative electrode in lithium ion batteries to deliver a reversible capacity of 400 mA h g^{-1} after repeated cycling.

Keywords Solvothermal synthesis · Tin oxide composite · Self-supporting electrode · Flexible electrode · Graphene

1 Introduction

Lithium ion batteries (LIBs) are currently the most popular rechargeable battery on the market, although they still suffer from problems such as safety, improper charge/discharge rates, and undesirable capacities for many applications such as electric vehicles [1, 2]. Currently commercial LIBs use graphite as the negative electrode active material, which has issues with low theoretical capacity of 372 mA h g^{-1} compared to SnO_2 which has a theoretical capacity of 782 mA h g^{-1} [3–6]. This superior capacity, along with SnO_2 being relatively inexpensive compared to other electrode materials, non-toxic, and able to be recycled has, sparked a great interest in using it as a negative electrode material for LIBs [7].

However, SnO_2 presents limitations as a negative electrode material due to volume expansion/contraction of approximately 300 % during lithium intercalation/deintercalation, which pulverizes the electrode [5, 6]. Pulverization of the electrode causes electrical conductivity to be lost between itself and the current collector, as well as disturbance of the solid electrolyte interface (SEI), leading to fast capacity fading [8]. Approaches to reduce issues with volume expansion/contraction in SnO_2 electrodes include the synthesis of nanomaterials as well as the combination of these nanomaterials with carbon nanostructures. It has been reported that SnO_2 nanoparticles [9–12], nanowires [13–15], and nanotubes [16] improve the capacity retention by providing space between particles to expand without being pulverized. Combining these nanomaterials with carbon nanotubes (CNTs) [5, 11, 17–19], graphene nanosheets (GNSs) [9, 19–29], and/or amorphous carbon [20, 30–33] further improves capacity retention and rate of charge/discharge by maintaining electrical conductivity between nanoparticles and elevating stress due to volume expansion during lithium intercalation/deintercalation [8, 9, 18, 30, 34–37].

On the other hand, another way to improve the energy density of LIBs is by removing and/or reducing the amount of electrochemical inactive materials used in the electrodes. Therefore, the negative electrode's electrochemical and physical properties can be enhanced by removing polymer binders and metal current collectors, and synthesizing self-supporting electrodes [8, 11, 38–45]. This modification to the electrode increases specific mass capacity of LIBs by

A. N. Gildea · D. Wang · G. G. Botte (✉)
Department of Chemical and Biomolecular Engineering, Center for Electrochemical Engineering Research, Ohio University, 182 Mill Street, Athens, OH 45701, USA
e-mail: botte@ohio.edu

removing inactive materials form the electrode that increases the mass of the cell, but not the capacity. Also, self-supporting electrodes generally have an increase in the mechanical flexibility of the electrode, as well as its electrical conductivity due to the removal of non-conductive polymer binders [41, 42, 46]. Free-standing binder-free conductive papers can be created by simple filtration of graphene oxide (GO) nanosheets (followed by either chemical or thermals reduction) or GNS dispersion through a micro porous membrane [42–44, 47]. This filtration technique creates strong and flexible uniform GNS film, which can be used directly in LIBs as a negative electrode, but has problems with low capacity of around 100 mA h g^{-1} [43–45]. Although it has been reported that the capacity of the GNS paper is low, the graphene paper exhibits a high conductivity ranging from 118 to 351 S cm^{-1} depended on the synthesis/post-treatment conditions [44, 48].

The improvement in electrical conductivity allows faster electron transport to the active material, which in turn increases the charge/discharge rate of the electrode [18, 42]. Polymer binders can also have poor adhesion of metal oxides, leading to fast capacity fading, compared to metal oxide nanoparticles anchored onto GNSs [42]. Another reason for removing metal current collectors from LIBs, besides decreasing the mass of inactive material, is that during battery cycling it becomes passivated, which decreases the lifetime and capacity of the LIBs [49]. Therefore removing metal current collectors not only increases the specific mass capacity of the cell, but also extends the lifetime of LIBs.

In this paper a dual prompt approach is taken to attempt a capacity increase in the anode electrode by combination of SnO_2 nanoparticles with GNS and amorphous carbon. A novel self-supporting binder-free SnO_2/GNS composite electrode is synthesized and evaluated for use as a negative electrode in LIBs. The synthesis of this material is accomplished using vacuum filtration of GO nanosheet dispersion through a micro porous membrane to make GO paper. This GO paper then undergoes simultaneous deposition of carbon coated SnO_2 nanoparticles onto its surface and chemical reduction of the GO paper to GNS film using a solvothermal technique. This material was characterized using X-ray diffraction (XRD), Scanning Electron Microscopy (SEM), Atomic Force Microscopy (AFM), Raman spectroscopy, Energy-dispersive X-ray spectroscopy (EDX), cyclic voltammetry, and constant current galvanic cycling.

2 Experimental

2.1 Material synthesis

GO nanosheets were prepared with the modified Hummers' method [50]. Then 0.3 g of the GO nanosheet powder was dissolved into 100 ml of DI water and ultrasonicated for 30 min (Zenith Ultrasonicator, 800 Watt, model # G2-40). The GO dispersion was centrifuged (Thermo Scientific, Sorvall Legend XI) at 4,000 rpm for 10 min. After the centrifuge, 10 ml of the dispersion was passed through a 0.22 μm Durapore membrane filter (47 mm diameter) under vacuum. After 3 h, all the solution was strained through the filter leaving a light brown film on the filter membrane. The Durapore membrane and the GO film were then dried under natural convection at room temperature for 8 h. Once the GO film was dried it was carefully peeled off the filter membrane, leaving a strong flexible translucent brown film.

A Tin (IV) chloride solution was prepared by dissolving 2.5 g of $SnCl_4{\cdot}5H_2O$ (98+ wt%, Acros Organics) into 20 ml of absolute ethanol (99.5 wt%, Acros Organics). 60 ml of an ethanol water mixture (40 ml absolute ethanol mixed with 20 ml of demonized water) was then added to the solution dropwise under vigorous stirring. The final mixture was then cooled to 0 °C for at least 6 h, and warmed to room temperature before 1.5 g of glucose (ACS reagent, anhydrous) was added [11].

Amorphous carbon coated SnO_2 nanoparticles were loaded onto the GO paper by a solvothermal method. A 2 × 4 cm piece of GO paper was loaded into a 50 ml Teflon autoclave vessel with 30 ml of the tin (IV) chloride solution prepared above. The autoclave vessel and the solution were then heated to 180 °C for 6 h. After this time the film was removed from the solution and thoroughly washed with DI water. The film change from light brown translucent color to a dark brownish black and became opaque. In this process, amorphous carbon and SnO_2 was coated onto the surface of the GO paper and the GO paper was reduced to GNSs.

The GO paper was chemically reduced to GNS film using 55 wt% hydriodic acid (HI, Sigma-Aldrich) [46]. This was accomplished by loading ½″ GO discs into a sealed 50 ml autoclave vessel with 10 ml of HI. The autoclave vessel was then heated to 100 °C for 12 h. The resulting GNS film was thoroughly washed with DI water and dried in a vacuum oven at 50 °C for 8 h.

2.2 Material characterization

The synthesized materials were characterized using XRD, AFM, Raman Spectroscopy, SEM, EDX, and four-probe electrical conductivity measurements. XRD analysis was performed on a Rigaku Ultima IV X-Ray Diffractometer with monochromatic Cu Kα radiation ($\lambda = 0.15405$ nm) at a scan rate of 2° min^{-1}. The AFM images were taken at room temperature under ambient conditions using Agilent Technologies 5500 AFM in AC mode with NSC15/AlBS probes from MikroMasch USA (Wilsonville, OR). AFM

samples were prepared by spin-coating 20 µl of graphene oxide dispersion onto a piece of freshly cleaved mica. Raman spectroscopy was accomplished on a Bruker Senterra Raman spectrometer. SEM was conducted on a JEOL-JSM-639OLV, with EDX attachment. The electrical conductivities were measured with a standard four-probe technique under ambient conditions using tungsten probe tips on an Agilent 34401A digital multimeter.

2.3 Electrochemical evaluation

All electrochemical tests were performed using a three-electrode t cell. SnO_2/GNS film or GNS paper was used as the working electrode, and lithium foil (99 wt%, MTI Corporation) was used as the counter and reference electrode. The working electrodes were separated from the lithium foil using a Celgard 2500 polyethylene separator. The electrolyte used for all of the experiments was 1 M lithium hexafluorophosphate in a mixture of ethylene carbonate and dimethyl carbonate 1:1 mass ratio (LP 40, BASF). All cells were assembled inside an argon filled glove box (MBraun UNIlab), H_2O and O_2 concentrations were maintained below 1 ppm. Discharge/Charge (D/C) tests along with cyclic voltammograms (CV) were performed using an 8 channel Solarton 1470E. D/C tests were performed at 100 mA g^{-1} normalized applied currents from 3.00 to 0.01 V versus Li/Li^+. CVs were scanned form 3.00 to 0.01 V versus Li/Li^+ at a scan rate of 0.1 mV s^{-1}.

3 Results and discussion

3.1 Characterization of GO, GNS, and SnO_2/GNS film

The dispersion of graphene oxide nanosheets was investigated by Atomic Force Microscopy (AFM). As shown in Fig. 1 a, the graphene oxide nanosheets are individually dispersed and the corresponding height measurements (Fig. 1b) show that the graphene oxide sheets have typical thickness of ~1 nm. The structural properties of the GO, GNS, and SnO_2/GNS films where characterized using Raman spectroscopy. Figure 2 reveals a D-band at ~1,345 cm^{-1} and G-band at ~1,570 cm^{-1} for GO, GNS, and SnO_2/GNS films, indicating the presence of carbon species in all the films. The increase in the ratio of D-band intensity (I_D) to G-band intensity (I_G) indicates that there is more sp^2 bonded carbon with smaller crystalline regime [51], which is caused by the removal of oxygen containing groups on the basal plane and edges of the GO nanosheets during chemical reduction. The I_D/I_G ratios for both SnO_2/GNS film (1.00) and pure GNS film (1.20) are larger than GO (0.92), providing evidence that both films were reduced. The smaller I_D/I_G ratio for the SnO_2/GNS film

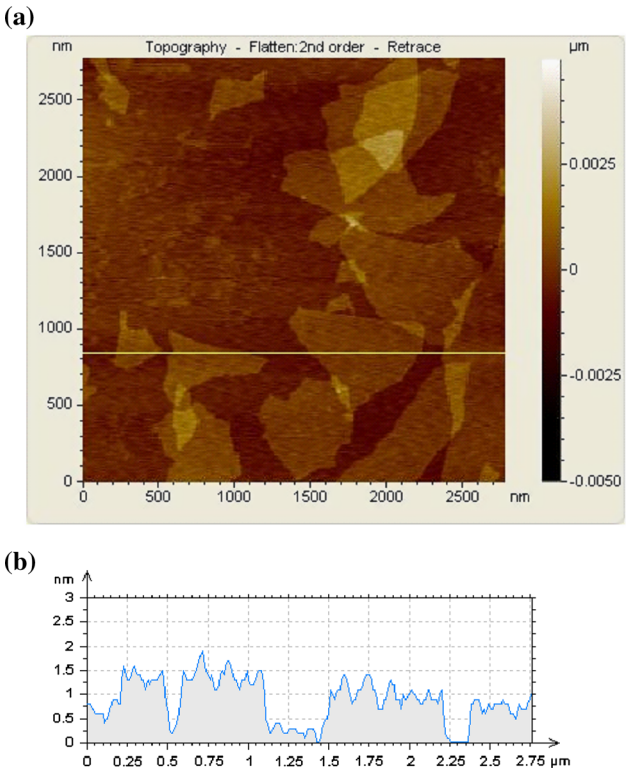

Fig. 1 **a** AFM image of graphene oxide nanosheets; **b** height measurements of graphene oxide nanosheets. The AFM image and height profile indicate the graphene oxide nanosheets are individually dispersed

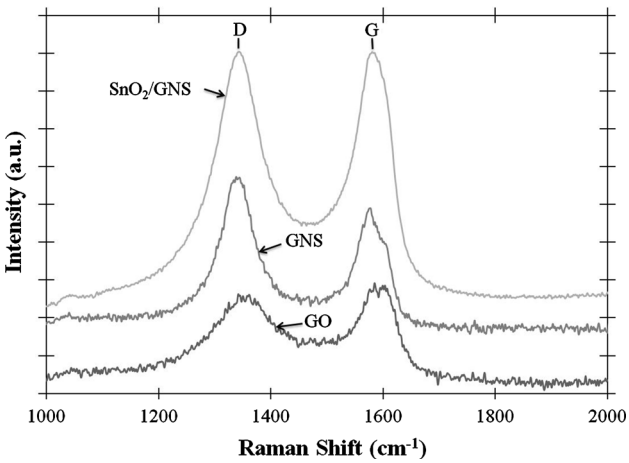

Fig. 2 Raman spectra of the GO, GNS, and SnO_2 films. All of these films exhibit D and G bands, demonstrating they are comprised of carbonaceous materials. The difference in peak intensities compared to GO paper indicates that the GNS and the SnO_2/GNS films are reduced

compared to the GNS film is due to the addition of the amorphous carbon coating on the surface of the GNS film, which adds significantly more sp^3 bonded carbon. Even though the I_D/I_G ratio for SnO_2/GNS film was lower than

pure GNS film, it still was larger than the GO paper, indicating that the solvothermal treatment reduces the GO paper to GNS film.

XRD patterns for GO paper, GNS film, SnO_2 powder, and SnO_2/GNS film are displayed in Fig. 3a. The diffraction pattern of SnO_2 powder reveals that SnO_2 is present in tetragonal crystalline structure (Cassiterite, JCPDS: 00-041-1445 Fig. 3b). The SnO_2/GNS film displays many of the same peaks as the SnO_2 powder, except that the peak at 26.4° for the SnO_2 is shifted to 25.8° and intensified. This is due to the overlap of the peak caused by the GNS film and the SnO_2 nanoparticles. Using the Scherrer's equation, the particle size of SnO_2 powder and SnO_2 particles deposited on the GNS film were estimated to be between 4 and 12 nm in diameter. The GNS film displays a sharp peak at 24.0°, while the GO paper reveals a sharp peak at 11.6°, which can be correlated to interlayer spacing between the individual GO nanosheets and GNSs using Bragg's Equation. The interlayer spacing has reduced from 0.77 nm for GO nanosheets to 0.38 nm for GNSs, which is due to the removal of oxygen containing groups located on the surface and edges of the GO nanosheets. It can also be seen that the GO peak disappears in the spectrum for the SnO_2/GNS film, demonstrating that the GO film was reduced during the solvothermal process, which is in agreement with the Raman spectroscopy results.

The SEM images of SnO_2/GNS film (Fig. 4), along with the EDX analysis of the film (Table 1), demonstrate how the SnO_2 and amorphous carbon was deposited onto the surface of the GNS film. The surface of the GNS film is

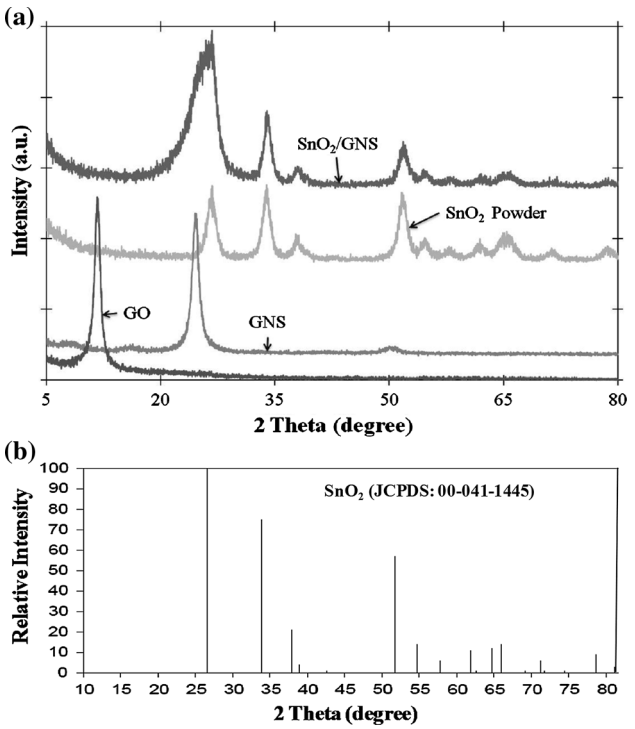

Fig. 3 **a** X-ray diffraction spectra of GO, GNS, and SnO_2/GNS films and SnO_2 powder. The spectra indicate that the GO paper is coated with SnO_2 nanoparticles and that the GO paper is reduced to GNS film; **b** the standard XRD pattern of SnO_2 (JCPDS: 00-041-1445)

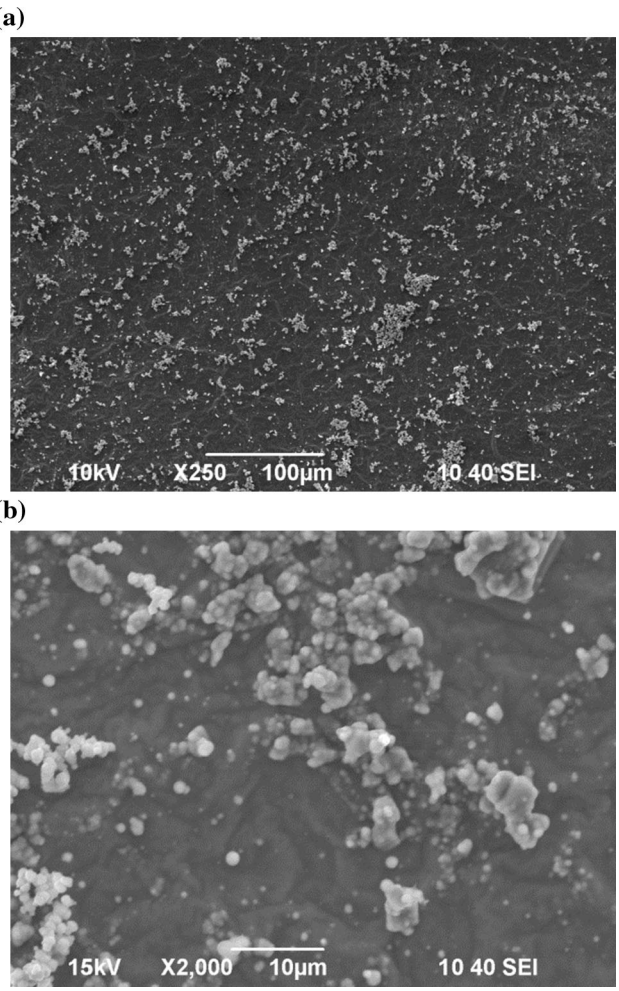

Fig. 4 SEM images of SnO_2/GNS film at **a** ×250 and **b** ×2,000 magnification. Lighter nodal growths on a darker wrinkled surface can be seen. Both the nodal growth and darker surface contain SnO_2 and carbon (determined by EDX analysis)

Table 1 EDX analysis of 4 SnO_2/GNS film surfaces at multiple magnifications from ×50 to 500

Elements	Weight (%)	Std	Atomic (%)	Std
C	39.96	2.76	74.31	1.72
O	11.87	0.11	16.61	0.74
Sn	48.17	2.80	9.10	0.97

This analysis quantifies the SnO_2 concentration in the film and demonstrates that the entire surface of the film is coated in SnO_2 and amorphous carbon

covered in an even coating of SnO_2 and amorphous carbon, which is seen from the images in Fig. 4a and b as a darker background. This darker coating has many wrinkles, which is indicative of the GNS substrate on which it is deposited. The SnO_2 amorphous carbon layer increases the reversible capacity of the electrode, but greatly decreases the electrical conductivity from 169 S cm^{-1} for GNS film to 0.011 S cm^{-1} for the SnO_2/GNS composite film due to the intrinsic property of oxide semiconductor.

From both Fig. 4a and b, it is observed that there are lighter nodal growths protruding from the darker surface. These nodal growths are comprised of many smaller nodes that range in size from about 1 to 10 μm, and are expected to contain agglomerations of SnO_2 nanoparticles held together by an amorphous carbon coating. Using EDX to analyze the surface of the electrode at magnification in a range of ×50–500 revealed that the surface contained only carbon, oxygen, and tin. The atomic percent and weight percent along with standard deviation found from analyzing multiple samples are given in Table 1. The darker background surface and the nodal growths were also analyzed individually to reveal that the nodal growths have a higher SnO_2 concentration and a lower carbon concentration compared to the darker background surface. Both the surface and the nodes contained tin, oxygen, and carbon indicating that the entire surface was coated in an amorphous carbon SnO_2 layer.

Using the weight percent found from the EDX analysis and the theoretical capacities of carbon (372 mA h g^{-1}) and SnO_2 (782 mA h g^{-1}) a theoretical capacity for the SnO_2/GNS film electrode was calculated to be 618 mA h g^{-1}. The amount of amorphous carbon and graphene carbon is unknown; therefore it was assumed that the two types of carbon are present in equal parts. In order to calculate the theoretical capacity of carbon present in the SnO_2/GNS film the average of the theoretical capacity of amorphous carbon (186 mA h g^{-1}) and graphene carbon (744 mA h g^{-1}) was used. Theoretically the GNS film should provide higher capacity than the SnO_2/GNS electrode, but experimentally the GNS film electrodes have given low reversible capacities of only around 100 mA h g^{-1} at low applied currents [43, 44].

3.2 Electrochemical evaluation of SnO_2/GNS film electrode

Cyclic voltammogram of the SnO_2/GNS film electrode is presented in Fig. 5. The electrochemical interaction with SnO_2 and carbon species can be described by the following chemical equations [5, 10, 20, 32, 35]:

$$4Li^+ + SnO_2 + 4e^- \rightarrow Sn + 2Li_2O \quad (1)$$

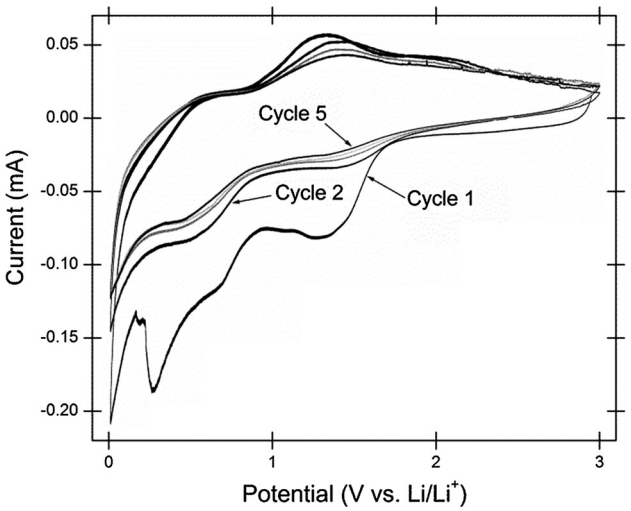

Fig. 5 Cyclic voltammogram of SnO_2/GNS film electrode at a scan rate of 0.1 mV s^{-1}. The first cycle shows irreversible reduction peaks due to the formation of the SEI layer and reduction of SnO_2 to Sn. Following cycles show reversible electrochemical reactions corresponding to lithium intercalation into carbon and Sn

$$xLi^+ + Sn + xe^- \rightarrow Li_xSn \quad 0 \leq x \leq 4.4 \quad (2)$$

$$yLi^+ + C + ye^- \rightarrow Li_y \quad 0 \leq y \leq 4.4 \quad (3)$$

During the first cycle there was a large irreversible reduction peaks at 1.4 V versus Li/Li^+ and 0.2 V versus Li/Li^+. The first irreversible reduction peak at 1.4 V versus Li/Li^+ can be attributed to the formation of the SEI layer on the surface of the electrode, while the second irreversible reduction peak at 0.2 V versus Li/Li^+ is caused by the reduction of SnO_2 to Sn (Eq. 1). These irreversible peaks disappear after the first cycle and reversible redox pairs are seen at 1.5 and 0.01–0.5 V versus Li/Li^+ in the following four cycles. The first redox pair 1.5 V versus Li/Li^+ can be attributed to the lithium ions intercalating into Sn (Eq. 2) which was formed in the first cycle. The last reversible redox pair located at 0.01–0.5 V versus Li/Li^+ is caused by the lithium insertion into carbonaceous species (Eq. 3) present in the SnO_2/GNS film. These results are similar to previously reported cyclic voltammograms of SnO_2 carbon composite materials [5, 19, 35].

Constant current galvanic cycling was performed at a constant normalized discharge rate of 100 mA g^{-1} or a C/6 rate. D/C curves of the SnO_2/GNS film for the first three cycles and the 40th cycle are displayed in Fig. 6a. These D/C curves are in good agreement with the CV discussed in the previous section, where during the first discharge there is a relatively large amount of irreversible capacity loss due to the formation of the SEI layer and the reduction of SnO_2 to Sn. Figure 6b displays discharge and charge capacity, as well as the Coulombic efficiency of the SnO_2/GNS film electrode at a constant normalized current of 100 mA g^{-1}

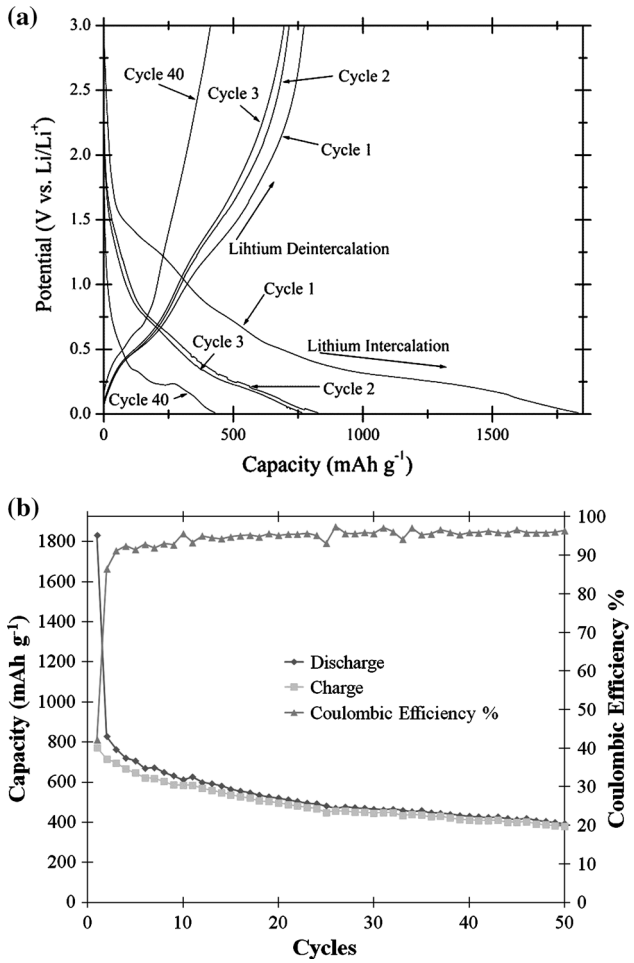

Fig. 6 Constant current galvanic cycling of SnO_2/GNS film electrode, normalized 100 mA g^{-1} (C/6) showing **a** discharge/charge curve for the first three cycles and 40th cycle and **b** the reversible capacity and Columbic efficiency as a function of cycle number. The discharge/charge curves reveal the voltage plateau regions and how the curves change with cell cycling. From **b** it can seen that the capacity fades and Columbic efficiency increases with cell cycling

as a function of cycle number. The first discharge (lithium intercalation) has a large capacity of $\sim$1,800 mA h g^{-1} and much smaller charge (lithium deintercalation) capacity of $\sim$800 mA h g^{-1} causing the first cycle to have a very low Coulombic efficiency of only 42 %. After the first cycle the Coulombic efficiency has already increased to 86 % and by the third cycle the Coulombic efficiency is maintained above 90 % for the remainder of the cell cycling. As cycle number increased the capacity begins to fade, with the biggest capacity fade occurring in the first 20 cycles. This capacity fading is due to the large volume expansion/contraction of Sn during lithium intercalation/deintercalation, which was discussed in the introduction. After 50 cycles the reversible capacity retention for the SnO_2/GNS film electrode has stabilized at $\sim$400 mA h g^{-1}. This novel electrode show much better capacity retention than plain SnO_2

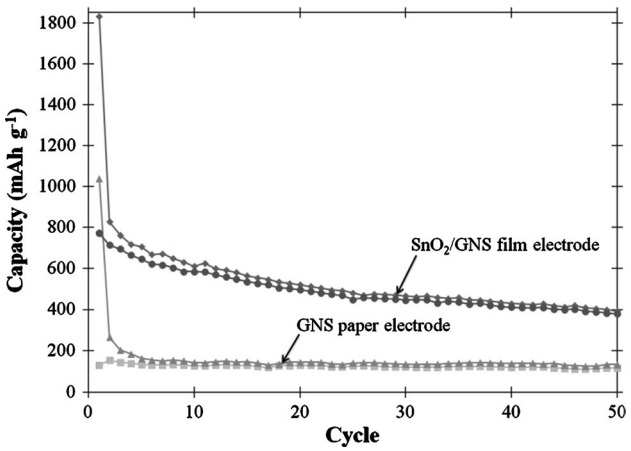

Fig. 7 Comparison of the reversible discharge capacities of the SnO_2/GNS film electrode and the GNS paper electrode at a constant normalized current of 100 mA g^{-1} for 50 cycles. Reversible capacity improves due to the addition of SnO_2 on the surface of the GNS film

nanoparticle electrodes and comparable capacity retention as previously reported SnO_2 carbon composite electrodes that use polymer binders and metal current collectors [4, 19–24, 31, 35, 36].

The reversible capacity of the GNS film and the SnO_2/GNS film electrodes are compared in Fig. 7. It can be seen that the GNS film electrode exhibits almost no capacity fading after the first few cycles, but has a much lower reversible capacity of only around 120 mA h g^{-1}, which is consistent with previous reports of GNS film used as electrode for lithium cells [43–45]. So in comparison, the addition of the carbon coated SnO_2 nanoparticles onto the surface of the GNS film adds approximately an additional 280 mA h g^{-1} to the self-supporting electrode, which is over a two hundred percent increase in the reversible capacity of the GNS paper. Also the capacity retention of the SnO_2 was greatly enhanced by the addition of carbonaceous materials in comparison against previously reported bare SnO_2 electrodes [19, 21, 24, 31, 35, 36].

4 Conclusion

In conclusion a flexible self-supporting binder-free SnO_2/GNS film electrode was synthesized using a simple and fast one-step solvothermal treatment of GO paper. This SnO_2/GNS film electrode was able to deliver 400 mA h g^{-1} reversible capacities after repeated cycling. The capacity is comparable with previously reported graphene/SnO_2 composite electrodes [23], but lower than graphene/confined SnO_2 electrodes, such as SnO_2 nanosheets/graphene electrode [23], atomic layer deposited SnO_2 with controlled morphology [10]. The capacity is also lower than ternary electrodes, such as Sn/CNT/graphene composite electrodes

[18]. Although the capacity of the SnO_2/GNS film electrode was lower than these confined SnO_2 carbon composite materials, it doesn't require conductive additives, polymer binders, or metal current collectors, which can account for around 50 % of the mass of the electrode. Also removing polymer binders, conductive fillers, and metal current collectors improves mechanical flexibility, electrical conductivity, and lifetime of LIBs. These improvements to the negative electrode permit greater application in new devices that require larger capacities and mechanical flexibility.

Acknowledgments The authors would like to thank the financial support of the Chemical and Biomolecular engineering department and the Center for Electrochemical Engineering Research at Ohio University.

References

1. Hossain S (1984) Rechargeable lithium batteries (ambient temperature). In: Linden D (ed) Handbook of batteries, vol 30, 2nd edn. McGraw-Hill Inc, New York, pp 36.31–36.44
2. Doughty D, Roth PE (2012) A general discussion of Li ion battery safety. Electrochem Soc Interface 21(2):37–44
3. Bruce PG, Scrosati B, Tarascon JM (2008) Nanomaterials for rechargeable lithium batteries. Angew Chem Int Ed 47(16): 2930–2946
4. Chen CM, Zhang Q, Huang JQ, Zhang W, Zhao XC, Huang CH, Wei F, Yang YG, Wang MZ, Su DS (2012) Chemically derived graphene-metal oxide hybrids as electrodes for electrochemical energy storage: pre-graphenization or post-graphenization? J Mater Chem 22(28):13947–13955
5. Li J, Zhao Y, Wang N, Guan L (2011) A high performance carrier for SnO_2 nanoparticles used in lithium ion battery. Chem Commun 47(18):5238–5240
6. Zhu X, Zhu Y, Murali S, Stoller MD, Ruoff RS (2011) Reduced graphene oxide/tin oxide composite as an enhanced anode material for lithium ion batteries prepared by homogenous coprecipitation. J Power Sour 196(15):6473–6477
7. U.S. Department of Health and Human Services (2005) Production, import/export, use, and disposal. In: Toxicological profile for tin and tin compounds. Agency for toxic substances and disease registry. U.S. Department of Health and Human Services, Washington, DC, pp 243–248
8. Tao HC, Fan LZ, Mei Y, Qu X (2011) Self-supporting Si/reduced graphene oxide nanocomposite films as anode for lithium ion batteries. Electrochem Commun 13(12):1332–1335
9. Chen Z, Zhou M, Cao Y, Ai X, Yang H, Liu J (2012) In situ generation of few-layer graphene coatings on SnO_2-SiC core-shell nanoparticles for high-performance lithium-ion storage. Adv Energy Mater 2(1):95–102
10. Li X, Meng X, Liu J, Geng D, Zhang Y, Banis MN, Li Y, Yang J, Li R, Sun X, Cai M, Verbrugge MW (2012) Tin oxide with controlled morphology and crystallinity by atomic layer deposition onto graphene nanosheets for enhanced lithium storage. Adv Funct Mater 22(8):1647–1654
11. Zhang HX, Feng C, Zhai YC, Jiang KL, Li QQ, Fan SS (2009) Cross-stacked carbon nanotube sheets uniformly loaded with SnO_2 nanoparticles: a novel binder-free and high-capacity anode material for lithium-ion batteries. Adv Mater 21(22):2299–2304
12. Szabo DV, Kilibarda G, Schlabach S, Trouillet V, Bruns M (2012) Structural and chemical characterization of SnO_2-based nanoparticles as electrode material in Li-ion batteries. J Mater Sci 47(10):4383–4391
13. Kim JH, Khanal S, Islam M, Khatri A, Choi D (2008) Electrochemical characterization of vertical arrays of tin nanowires grown on silicon substrates as anode materials for lithium rechargeable microbatteries. Electrochem Commun 10(11): 1688–1690
14. Park MS, Wang GX, Kang YM, Wexler D, Dou SX, Liu HK (2007) Preparation and electrochemical properties of SnO_2 nanowires for application in lithium-ion batteries. Angew Chem Int Ed 46(5):750–753
15. Xia X, Li S, Wang X, Liu J, Wei Q, Zhang X (2013) Structures and properties of SnO_2 nanofibers derived from two different polymer intermediates. J Mater Sci 48(9):3378–3385
16. Wang J, Du N, Zhang H, Yu J, Yang D (2011) Large-scale synthesis of SnO2 nanotube arrays as high-performance anode materials of Li-ion batteries. J Phys Chem C 115(22): 11302–11305
17. Liu H, Huang J, Li X, Liu J, Zhang Y (2012) One-step hydrothermal synthesis of flower-like SnO_2/carbon nanotubes composite and its electrochemical properties. J Sol-Gel Sci Technol 63(3):569–572
18. Zou Y, Wang Y (2011) Sn@CNT nanostructures rooted in graphene with high and fast Li-storage capacities. ACS Nano 5(10):8108–8114
19. Chen T, Pan L, Liu X, Yu K, Sun Z (2012) One-step synthesis of SnO_2-reduced graphene oxide-carbon nanotube composites via microwave assistance for lithium ion batteries. R Soc Chem Adv 2(31):11719–11724
20. Wen Z, Cui S, Kim H, Mao S, Yu K, Lu G, Pu H, Mao O, Chen J (2012) Binding Sn-based nanoparticles on graphene as the anode of rechargeable lithium-ion batteries. J Mater Chem 22(8): 3300–3306
21. Sathish M, Mitani S, Tomai T, Unemoto A, Honma I (2012) Nanocrystalline tin compounds/graphene nanocomposite electrodes as anode for lithium-ion battery. J Solid State Electrochem 16(5):1767–1774
22. Sathish M, Mitani S, Tomai T, Honma I (2012) Ultrathin SnS_2 nanoparticles on graphene nanosheets: synthesis, characterization, and Li-ion storage applications. J Phys Chem C 116(23):12475–12481
23. Luo B, Wang B, Li XL, Jia YY, Liang MH, Zhi LJ (2012) Graphene-confined Sn nanosheets with enhanced lithium storage capability. Adv Mater 24(26):3538–3543
24. Wang G, Wang B, Wang X, Park J, Dou S, Ahn H, Kim K (2009) Sn/graphene nanocomposite with 3D architecture for enhanced reversible lithium storage in lithium ion batteries. J Mater Chem 19(44):8378–8384
25. Jiang S, Yue W, Gao Z, Ren Y, Ma H, Zhao X, Liu Y, Yang X (2013) Graphene-encapsulated mesoporous SnO_2 composites as high performance anodes for lithium-ion batteries. J Mater Sci 48(10):3870–3876
26. Lian P, Wang J, Cai D, Ding L, Jia Q, Wang H (2014) Porous SnO_2@C/graphene nanocomposite with 3D carbon conductive network as a superior anode material for lithium-ion batteries. Electrochim Acta 116(10):103–110
27. Zhu J, Wang D, Wang L, Lang X, You W (2013) Facile synthesis of sulfur coated SnO_2-graphene nanocomposites for enhanced lithium ion storage. Electrochim Acta 91(28):323–329
28. Zhao B, Zhang G, Song J, Jiang Y, Zhuang H, Liu P, Fang T (2011) Bivalent tin ion assisted reduction for preparing graphene/SnO_2 composite with good cyclic performance and lithium storage capacity. Electrochim Acta 56(21):7340–7346

29. Yue W, Yang S, Ren Y, Yang X (2013) In situ growth of Sn, SnO on graphene nanosheets and their application as anode materials for lithium-ion batteries. Electrochim Acta 92(1):412–420
30. Liang S, Zhu X, Lian P, Yang W, Wang H (2011) Superior cycle performance of Sn@C/graphene nanocomposite as an anode material for lithium-ion batteries. J Solid State Chem 184(6): 1400–1404
31. Wu P, Du N, Liu J, Zhang H, Yu J, Yang D (2011) Solvothermal synthesis of carbon-coated tin nanorods for superior reversible lithium ion storage. Mater Res Bull 46(12):2278–2282
32. Qiao H, Zheng Z, Zhang L, Xiao L (2008) SnO_2@C core-shell spheres: synthesis, characterization, and performance in reversible Li-ion storage. J Mater Sci 43(8):2778–2784
33. Li X, Zhong Y, Cai M, Balogh MP, Wang D, Zhang Y, Li R, Sun X (2013) Tin-alloy heterostructures encapsulated in amorphous carbon nanotubes as hybrid anodes in rechargeable lithium ion batteries. Electrochim Acta 89(1):387–393
34. Magasinski A, Dixon P, Hertzberg B, Kvit A, Ayala J, Yushin G (2010) High-performance lithium-ion anodes using a hierarchical bottom-up approach. Nat Mater 9(4):353–358
35. Yao J, Shen XP, Wang B, Liu H, Wang GX (2009) In situ chemical synthesis of SnO_2–graphene nanocomposite as anode materials for lithium-ion batteries. Electrochem Commun 11(10):1849–1852
36. Zhong C, Wang J, Chen Z, Liu H (2011) SnO_2-graphene composite synthesized via an ultrafast and environmentally friendly microwave autoclave method and its use as a superior anode for lithium-ion batteries. J Phys Chem C 115(50):25115–25120
37. Hassan FM, Chen Z, Yu A, Chen Z, Xiao X (2013) Sn/SnO_2 embedded in mesoporous carbon nanocomposites as negative electrode for lithium ion batteries. Electrochim Acta 87(1): 844–852
38. Wang D, Kou R, Choi D, Yang Z, Nie Z, Li J, Saraf LV, Hu D, Zhang J, Graff GL, Liu J, Pope MA, Aksay IA (2010) Ternary self-assembly of ordered metal oxide-graphene nanocomposites for electrochemical energy storage. ACS Nano 4(3):1587–1595
39. Lee JK, Smith KB, Hayner CM, Kung HH (2010) Silicon nanoparticles-graphene paper composites for Li ion battery anodes. Chem Commun 46(12):2025–2027
40. Zhao X, Hayner CM, Kung MC, Kung HH (2011) In-plane vacancy-enabled high-power Si-graphene composite electrode for lithium-ion batteries. Adv Energy Mater 1(6):1079–1084
41. Liu F, Song S, Xue D, Zhang H (2012) Folded structured graphene paper for high performance electrode materials. Adv Mater 24(8):1089–1094
42. Gwon H, Kim HS, Lee KU, Seo DH, Park YC, Lee YS, Ahn BT, Kang K (2011) Flexible energy storage devices based on graphene paper. Energy Environ Sci 4(4):1277–1283
43. Abouimrane A, Compton OC, Amine K, Nguyen ST (2010) Non-annealed graphene paper as a binder-free anode for lithium-ion batteries. J Phys Chem C 114(29):12800–12804
44. Wang C, Li D, Too CO, Wallace GG (2009) Electrochemical properties of graphene paper electrodes used in lithium batteries. Chem Mater 21(13):2604–2606
45. Liu S, Chen K, Fu Y, Yu S, Bao Z (2012) Reduced graphene oxide paper by supercritical ethanol treatment and its electrochemical properties. Appl Surf Sci 258(13):5299–5303
46. Pei S, Zhao J, Du J, Ren W, Cheng H-M (2010) Direct reduction of graphene oxide films into highly conductive and flexible graphene films by hydrohalic acids. Carbon 48(15):4466–4474
47. Dikin DA, Stankovich S, Zimney EJ, Piner RD, Dommett GHB, Evmenenko G, Nguyen ST, Ruoff RS (2007) Preparation and characterization of graphene oxide paper. Nature 448(7152): 457–460
48. Chen H, Muller MB, Gilmore KJ, Wallace GG, Li D (2008) Mechanically strong, electrically conductive, and biocompatible graphene paper. Adv Mater 20(18):3557–3561
49. Myung ST, Hitoshi Y, Sun YK (2011) Electrochemical behavior and passivation of current collectors in lithium-ion batteries. J Mater Chem 21(27):9891–9911
50. Hummers WS, Offeman RE (1958) Preparation of graphitic oxide. J Am Chem Soc 80:1339
51. Ferrari AC, Robertson J (2000) Interpretation of Raman spectra of disordered and amorphous carbon. Phys Rev B 61(20): 14095–14107